We are IntechOpen, the world's leading publisher of Open Access books Built by scientists, for scientists

4,800
Open access books available

122,000
International authors and editors

135M
Downloads

Our authors are among the

154
Countries delivered to

TOP 1%
most cited scientists

12.2%
Contributors from top 500 universities

WEB OF SCIENCE™

Selection of our books indexed in the Book Citation Index in Web of Science™ Core Collection (BKCI)

Interested in publishing with us?
Contact book.department@intechopen.com

Numbers displayed above are based on latest data collected.
For more information visit www.intechopen.com

23

Isotope Effects Induced by Exterior Actions on the Solid Surface

Nikolay N. Nikitenkov, Yurii I. Tyurin and Vitalii V. Larionov
Tomck Polytechnical University
Russia

1. Introduction

Many scientific and technological problems for which solution the examination of the isotope composition or its modification as a result of certain processes are required. So, for example, in geology it is the problems related to geochronology, isotope geochemistry (including shaping of the earth crust, examination of a glaciers etc.). In the space researches: a problems of the isotope space geochemistry, the space chemistry and the space geochronology (processes of shaping of a planets, comets, asteroids; the history of shaping of a chemical elements in the Universe) (Shukolyukov Yu.A., 1996). In the nuclear power: the fuel and other functional materials of the nuclear and thermonuclear reactors. And many other things.

Now are known many processes in which a diversions from the natural abundances of isotopes are observed. In the physics and chemistry the following processes are most known:

a. The kinetics processes;
b. The reactions of the isotopic interchanging;

These processes are responsible for a isotope modifications in the following physical and chemical phenomena: evaporation, condensation, melting, crystallization, diffusion and dissociation.

Thus it is known, that chemical bonds with a heavy isotopes more strongly than the same bonds with a light isotopes.

In general terms, all isotopic effects can be parted on two types:

1. Kinetic - based on different velocities of processes and caused by the fact that in the aggregate of interacting molecules the particles with smaller mass possess greater velocity;
2. Thermodynamic - which are reflection of a different energy states of the system. A composition with heavy isotopes possesses a smaller reserve of a free energy, than the same compositions with a light isotope (Galimov E.M., 1981).

It is now know also that deriving of the large isotopic effect in certain process are necessary: a high relative odds of masses, a high degree of chemical bond covalence, modifications of a oxides states, a modification of a phase or modular state.

Last researches of isotopic effects in the chemistry have led to discovery of one more view of the isotopic effect - fractionation of nuclear-isotopes on a nuclear magnetic moment (Buhanchenko A.L., 2007). The possibility of detection of nuclear polarization is a new

research technique of mechanisms of a chemical reactions and it is a method of detection of a radicals and radical stages in a chemical process. The magnetic isotopic effect significantly differs by the nature from the usual kinetic isotopic effect related to difference in the isotope masses.

In condensed matter the isotope effects are manifested more brightly than in other states of matter.

Now the solid-state physics studies influence of isotope effects on elastic, thermal both vibrational and other properties of crystals. It is installed, for example, that at replacement of hydrogen on a deuterium in the LiH crystal the energies of a electron transitions increase by 2 orders (Plekhanov V.G., 2003). Now actual problems of isotope engineering are new medium for a data recording, a doping in a semiconductor by a neutron nuclear transmutation, control sensors betterment by ultrapure materials and many other things. Actual problem and major reaching in materials technology is the growing of crystals with the controlled isotope composition.

The purpose of the present chapter is a review of the latest work and new experimental data on changes in the isotope composition in the near-surface layers of solids as a result of the secondary ion emission, ion scattering from the surface, ion implantation, electrolytic saturation by hydrogen isotopes, thermo-diffusion from external sources and chemical solution action on the solid surface is presented. Such investigation is needed in materials technology, where atom migration mechanisms and isotope composition changes during various surface interactions occur. The change of isotope composition of the ion beams and near-surface layers of solids has been studied in many works on ion sputtering and secondary ion emission, scattering of ions from surfaces, hydrogen saturation and thermo diffusion from external sources and ion implantation. In all these phenomena, it is very important to identify the basic processes, which determine the change of isotope composition in the near-surface layers of solids.

The good understanding of physical mechanisms, which are reviewed here (and of others still unknown mechanisms) will become a basis for the obtaining of the monoisotopic or enriched surfaces with a certain isotopes. It, undoubtedly, will be claimed by future technologies. These investigations are also of the great academic interest as example of non-equilibrium systems.

2. Experimental results and discussion

2.1 Isotope effects during ion sputtering and the secondary ion emission

Slodzian et al were probably the first to study the isotope effect (IE) in secondary ion emission (SIE) (Slodzian et al, 1980), although preferential sputtering was noted earlier in 1977 (Lorin et al, 1982). It was established (Slodzian et al, 1980) that in SIE of some minerals, metals, copper oxide, and GaAl alloy produced by oxygen ions, in the energy range 0–20 eV the yield of the light isotope in comparison to the heavy one is greater than the natural isotope ratio. Thus, the enrichment of the sputtered particles by the light ions was found. The degree of enrichment depends on the isotope atomic number, on the matrix containing the isotope in question, and on the ion velocity. Almost at the same time, the space and energy distribution of the SIE isotope rate was studied (Shapiro et al, 1985). The data (Shapiro et al, 1985) confirmed the results and conclusions (Slodzian et al, 1980). The ratio $f_{LH}(E)=N^{+}_{L}(E)/N^{+}_{H}(E)$ for metals, (where $N^{+}_{L}(E)$ and $N^{+}_{H}(E)$ are the energy spectra of the secondary light and heavy ions) has been thoroughly studied. It was found that, in the ratio

$f_{LH}(E)$ in the energy range (0–80 eV) there is either peak or plateau at different energies for different metals. As a rule, this peak is located at low energies for the light elements and displaced to greater energies for the heavy ones.

The function $f_{LH}(E)$ in the energy range E=4–30 эВ was studied carefully (Gnaser & Hutcheon, 1987) to verify the proposed effect model. Lately IE in sputtering and SIE were studied too (Gnaser & Hutcheon, 1988), (Gnaser & Oechsner, 1990), (Shimizu & Hart, 1982), (Shapiro et al, 1985), (Shwarz, 1987). In order to explain isotope effect in SIE (IESIE), the standard ionization probability equations (Shapiro et al, 1985) and the experimental dependences of ionization probability on the atomic velocity (v) in the form of $\exp(-v_0/v)$ (v_0 is constant) are used. The change of the isotope composition follows from the dependence of ionization probability on atomic mass. However, it does not explain the mechanism of the phenomenon.

The experimental investigation of IESIE and its mechanism is the main object of our research (Nikitenkov et al, 1987, 1988) – the functions $f_{LH}(E)$ for metals somewhat similar to those described were studied. In general, our data confirm the results of previous work, although our experimental values for some metals are greater (Fig.1).

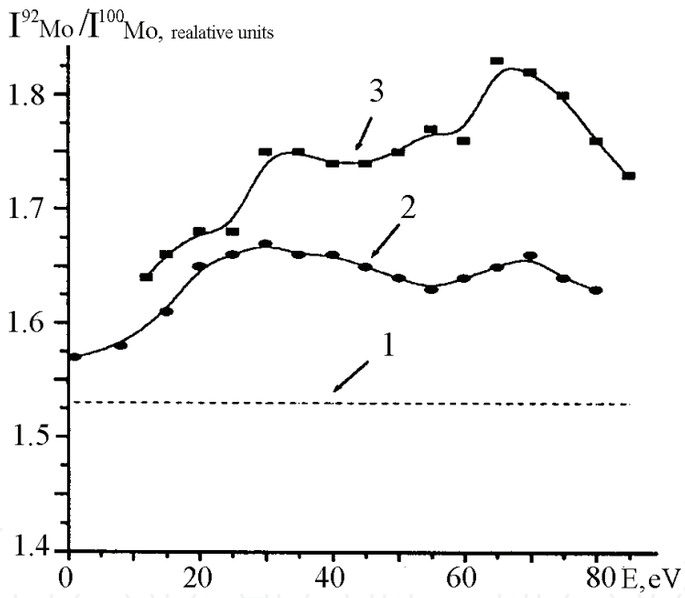

Fig. 1. The mass line intensity ratio of molybdenum ions 92 Mo and 100Mo as a function of energy: 1 – standard isotope ratio, 2 – (Shimizu & Hart, 1982) data, 3 – our data.

The experimental data confirm the existence of a peak or plateau in the $f_{LH}(E)$ function, although the correlation between the peak energy position and the isotope mass was not confirmed. At the same time, a decrease in the ratio of the maximum value $f_{LH}(E)$ to the natural abundance with decreasing isotope mass has been observed. It was also shown that the larger the nuclei neutron difference the greater is the IESIE.

From all established regularities, the most reliable are follows: there is the greater ionization probability of the light isotope in comparison with the heavy one, and there is an inverse dependence of the effect on atomic mass. The last dependence obviously correlates with the relative nuclear mass and volume change for the same deficit or excess of neutrons while moving from the light isotopes to the heavy ones. This fact shows that IESIE is due to the

difference in composition of atomic electron shells. This difference is due to the isotope displacement (ID) of the atomic electron energy levels. ID depends mainly on the nuclear mass and dimension.

The isotopic displacement of electron levels due to the nuclear dimensions is caused by overlapping of the s-electron and nucleus wave functions. The probability of electron localization in the nucleus volume becomes rather great (Gangrskiy & Markov, 1984). The nucleus size is described by the mean square (proton) radius $<r^2>$. Its value depends on the number of neutrons in the nucleus (Fig. 2). Thus, the nucleus size affects the atom ionization potential and consequently the atom ionization probability during the sputtering process. This influence can manifest itself through the ionization potential value and the interaction length (λ) between atoms and the surface. These quantities depend on $<r^2>$ (indeed $\lambda \sim a \sim <r^2>$, where a is the atom radius).

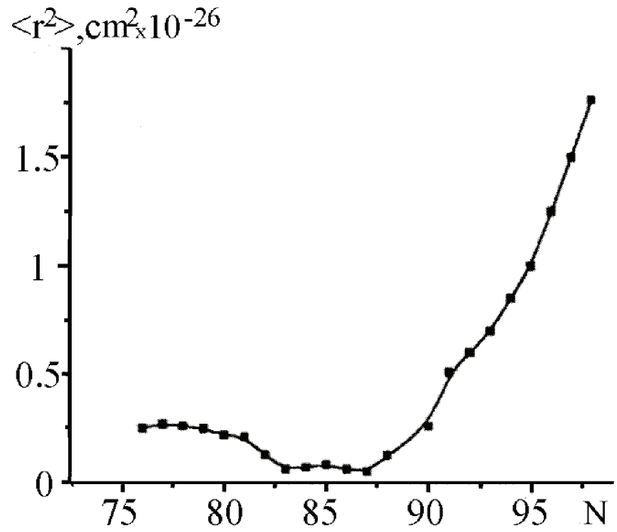

Fig. 2. The mean square nucleus radius as a function of the number of neutrons N for rubidium isotopes (Gangrskiy & Markov, 1984).

The isotope displacements of spectral line frequencies of some optical transitions are about 10^{-5}–10^{-4} eV. The ionization energy (I) of isotopes should differ with the ID values observed by optical experiments. The ionization probability at SIE depends on I exponentially. Thus, we can evaluate the relative difference in ionization probability for different isotopes. For example (Nikitenkov et al, 1987), the ionization probability R^+ may be:

$$R^+(E) \sim E^n \cdot \exp\left[-\frac{(I-\varphi)\cdot c}{E^{1/2}}\right], \tag{1}$$

E is the ion kinetic energy, I is the ionization energy, φ is work function, $c = \pi/2\gamma\hbar$, $\hbar = h/2\pi$ where h is Planck's constant; $n = \gamma_a\delta/4\gamma kT_s$, $\gamma_a = a_p/v$ is a quantity describing the interaction length between the surface and the escaping atom; a_p is a quantity of the lattice constant order; v is the velocity of the recoil atom; δ is a constant; k is the Boltzmann's constant; T_s is the temperature of an electron subsystem in the cascade developing region. With the help of the formula (1) we get the relative difference of ionization probabilities for two atoms with the potential increment ΔI and an interacting length increment $\Delta\lambda = \Delta(1/\gamma_a)$ as follows:

$$R(E)=\frac{R_1^+-R_2^+}{R_2^+}=\frac{R_1^+}{R_2^+}-1=E^{(\Delta\lambda)\cdot\kappa_1}\cdot\exp\left[\frac{\Delta I\cdot\kappa_2}{E^{1/2}}\right]-1 \quad (2)$$

here $\lambda=1/\gamma_a$, κ_1 and κ_2 are dimensional constants (previously we assumed $\kappa_1=\kappa_2=1$).
Fig. 3 shows experimental and theoretical curves designed with using equation (2) and the following relation:

$$R(E)=\frac{\Delta R^+}{R^+}=E^{\Delta\lambda}-1 \quad (3)$$

The formula (3) is obtained in an analogous way to formula (2) using the relation ($R^+\sim E^n$) instead of the formula (1). We assume that $\kappa_1\cdot\Delta\gamma\approx\kappa_2\cdot\Delta I\approx10^{-4}$. In addition, the curve 1 (Fig. 3) for ^{107}Ag and ^{109}Ag isotopes represents the experimental quantity:

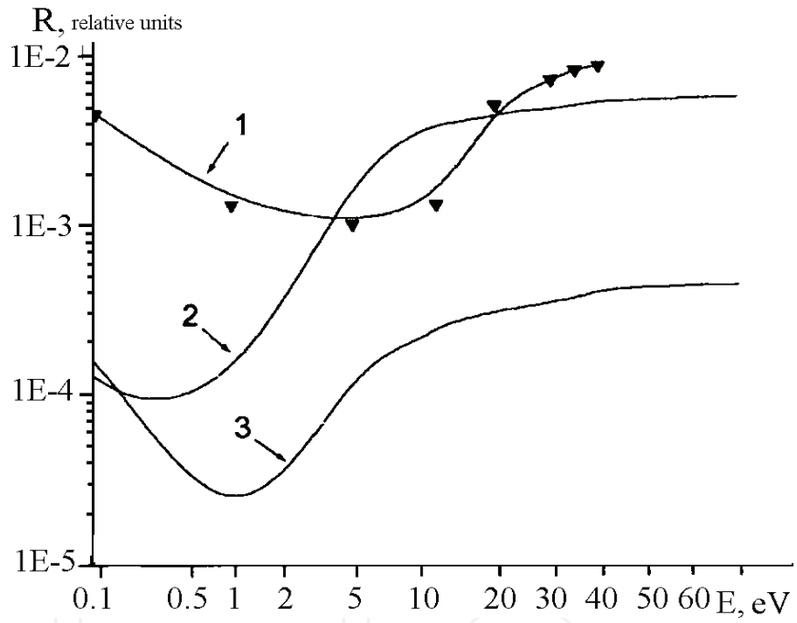

Fig. 3. Relative probabilities of ionization of the secondary ions as a function of energy:
1 – experimental data in accordance with formula (4);
2 and 3 – theoretical values in accordance with formulas (2) and (3).

$$R'(E)=\frac{\Delta M}{M}\cdot\left|\frac{R_{\text{exp.}}}{R_{st}}-1\right|, \quad (4)$$

here $R_{exp.}=I^+_L(E)\,/\,I^+_H(E)$, I_i^+ ($i=L,H$) are the isotope mass line intensities in corresponding energy spectra, R_{st} is the standard isotope ratio and $\Delta M/M$ is the relative mass difference.
Fig. 4 shows the quantities $R'(E)$ (4) for some isotopes obtained in our experiments (Fig. 4, a) and additional result of Shimizu et al (Fig. 4, b). A comparison of Fig. 3 and Fig. 4 leads to the conclusion that the form of every experimental curve corresponds (in general) to the theoretical curve. The experimental and theoretical (R and R') quantities are often close at the minima. The different positions of the sharp minima of the theoretical and experimental

curves can be explained by the experimental errors caused, in particular, by wide energy windows (about 1 eV) of the energy analyzers. Thus, the given results suggest a possible relation between IESIE and isotope shift of the ionization level of an atom.

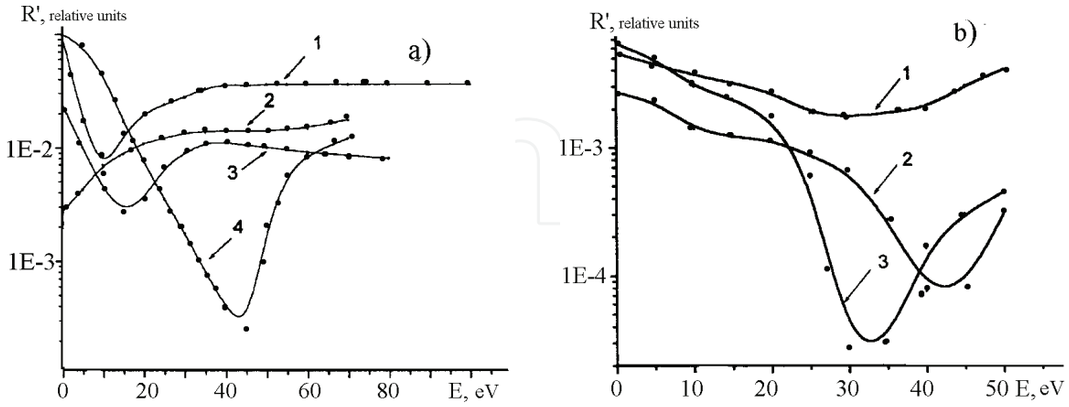

Fig. 4. The experimental quantities (R_{exp}/R_{st}) as a function of the secondary ion energy:
a – our data for: 1—^{24}Mg and ^{26}Mg, 2—^{92}Mo and ^{94}Mo, 3—^{50}Cr and ^{52}Cr, 4—^{114}Sn and ^{116}Sn;
b – data from (Shimizu & Hart, 1982). 1 —^{28}Si and ^{30}Si, 2—^{50}Cr and ^{52}Cr, 3—^{24}Mg and ^{26}Mg.

2.1.2 Isotope effects during ion scattering on surface

The isotope effects in the ion fluxes backscattered from metallic surfaces have been mainly studied for $^{3}He^{+}$–$^{4}He^{+}$ and $^{20}Ne^{+}$–$^{22}Ne^{+}$ ion pairs (Helbig & Orvek, 1980), (Helbig & Adelman, 1977). The method of ion scattering double spectroscopy (ISDS) was applied. When using this method, the components of the ion pairs are present in the primary beam in equal concentrations. A method of alternating injection of these isotopes in the discharge chamber was used. The energy of the primary ions was in the range 200–3000 eV, the electric current from 0.1 up 500 nA, the incident and reflect ion angles 0–180 degrees.

Fig. 5 shows the IE data for the $^{3}He^{+}$–$^{4}He^{+}$ pairs (Helbig & Adelman, 1977). The scattering yield (Y) is represented in arbitrary units, although the relative intensity difference of $^{3}He^{+}$–$^{4}He^{+}$ pairs for every metal corresponds to the experiment. The abscissa axis origin for every metal (Zn, Pb, In, Sn) is designated by the dashed line below the chemical symbol. The values of the reciprocal velocity ($1/v=m/2Ve$, where m and e are the ion mass and charge, V accelerating potential) are shown on the abscissa axis. A very appreciable maximum structure of the curves for lead, indium, and tin has been explained as the result of competition between the scattering cross section increase and changes in neutralization probability when decreasing the beam energy (Smith, 1971).

At small reverse velocity, the scattered $^{3}He^{+}$ ion current is greater than that of $^{4}He^{+}$ ions for all ion-target combinations. This is quite natural, because the scattering cross section of light particles is greater than that for heavy particles under identical conditions (the force field, neutralization probability). For all studied systems at high values of inverse velocity, the scattered $^{4}He^{+}$ ion current tends to be greater than that of $^{3}He^{+}$ ions. This is obviously due to the fact that, at low energy, the $^{4}He^{+}$ ions neutralize with appreciably less probability then that for the $^{3}He^{+}$ ions. The difference between these isotopes of the same velocity is caused by their different momenta, which, in its turn, leads to a small deviation (less then 1 Bohr unit) in their scattering trajectories. The basic neutralization processes (the Auger

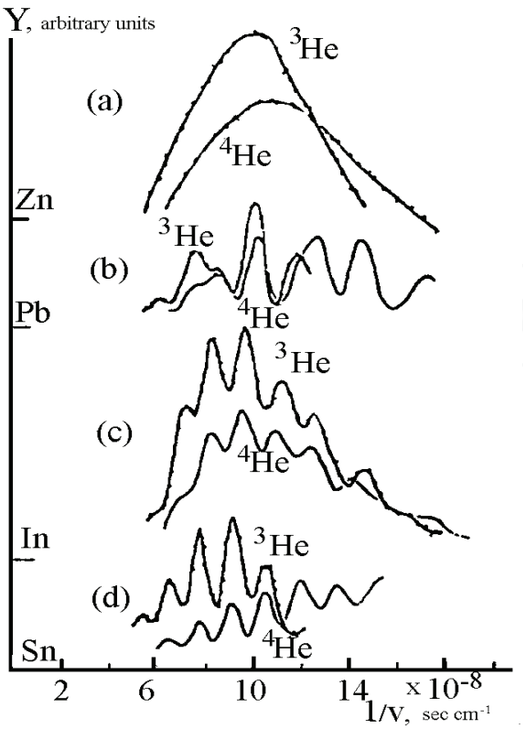

Fig. 5. The elastic scattered ion ^{3}He+ and ^{4}He+ yield (Y) as a function of inverse velocity for zinc, lead, indium, and tin surfaces; the scattering angle is 90°(Helbig & Adelman, 1977).

neutralization and resonance tunnel neutralization) are believed to occur rather far from the surface (about 4 Bohr units). It is difficult to understand why such small differences in their trajectories can affect the relative neutralization probability of these ionized isotopes.

Heavy ions produce greater modification of a surface than light ions in the processes of implantation, surface etching, and cleaning. However, these processes cannot be responsible for curves peculiarities at low energies.

The curve oscillations (Fig. 5) for helium ions scattered from lead, indium, and tin surfaces have been explained by quasi-resonance electron transportation (Erikson & Smith, 1975). A glance at these curves shows that the positions of maxima and minima for scattering of ^{3}He$^+$ and ^{4}He$^+$ ions from the same surface correspond to the identical inverse velocities (Erikson & Smith, 1975). However, a more detailed analysis leads to the conclusion that, in the low energy range, there are appreciable displacements of the maximum and minimum positions. While bombarding the lead surface (Fig. 5 c), the isotope shift (at the inverse velocity about $12 \cdot 10^{-8}$ sec·cm^{-1}) coincides with data for angular distributions (Erikson & Smith, 1975): i.e. increasing the scattering angle, at constant energy and mass of bombardment particles, leads to the same effects as increasing their mass at constant velocity and scattering angle. In both cases, the distance of maximum approach decreases. It is very interesting to note that the displacements of a low energy peak for indium and tin (Fig. 5 c, d) are of the opposite sign than those for the lead.

From Fig. 5 it follows that the heights of the ^{3}He$^+$ and ^{4}He$^+$ peaks are not identical and are not proportional each other. The differences of peak heights in the tin low energy spectra are probably due to the differences of the curve general form. The zinc non oscillatory data (Fig. 5, a) confirm this. In general, the curves have a parabolic form with a sinusoidal modulation.

About the possible reasons of such oscillations look (Tolk et al, 1976). The scattering $^{3}He^{+}$ from Pb is an exclusion from this rule. This curve has a small peak at the inverse velocity about $8{,}5 \cdot 10^{-8}$ sec·cm^{-1}, which is apparently due to the quasi-resonance electron transportation. The reflected light ion currents for $^{3}He^{+}$ and $^{4}He^{+}$ ions are about two times greater than those for heavy isotopes. For $^{20}Ne^{+}$ and $^{22}Ne^{+}$ ions, this increment is about 20 %, i.e. the heavier the isotope, the smaller the effect. It correlates with the isotope relative mass difference (just the same as for IE SIE). For a detailed explanation of ISDS energy distributions it is necessary (as well for SIE) to consider the ID of the ionization level.

2.1.3 Isotope effects during ion implanting

Our results on changing the isotope composition of copper, implanted in nickel, are represented in (Puchkareva et al, 2002). The ion implantation of copper atoms in the nickel polycrystals with average grain size about 20 micron has been produced by an implanter "Diana-2" (Aksenov, 1987) provided with a vacuum arc ion source in an impulse periodical regime with the impulse length 150–200 μs and frequency 50 Hz. The implantation was performed at the pressure $6 \cdot 10^{-3}$ and $4 \cdot 10^{-2}$ Pa at an ion impulse current density of 125 μA·cm^{-2} and average target current density of 1 μA·cm^{-2}. The implantation doses were $2 \cdot 10^{16}$ and $2 \cdot 10^{17}$ ion·cm^{-2}, the time interval for accumulating these doses was about 6 hours. The ions were accelerated to 50 kV. Previously electrochemically polished nickel samples were mounted upon a metallic support in such a way as to provide the tight contact with the metallic substrate surface. While implanting the sample the temperature was not more than 50 °C. Fig. 6 shows the distribution profiles for ^{65}Cu and ^{63}Cu through the nickel sample depth and the summed $^{65}Cu+^{63}Cu$ profile after implanting to a dose of $2 \cdot 10^{17}$ ion·cm^{-2} at a pressure of $6 \cdot 10^{-3}$ Pa. It is seen, that the isotope distribution patterns are different: a sloping curve for ^{65}Cu and a rising curve for ^{63}Cu. This means that, in the surface layer at a distance about 100 nm, the ^{65}Cu atoms have accumulated. After reaching the ^{63}Cu intensity line maximum, equalization of isotope composition begins, approaching a natural ratio at the depth 250 nm.

Fig. 6 and Fig. 7 show the depth concentration discrepancies for copper isotopes $C_i = I_i / \Sigma I_i$ (i – isotope, I – mass line intensity) to their natural abundances (R_i). At the depth of about 330 nm the data on isotope composition for implanted copper atoms coincide with the natural. A maximum deviation from the isotope natural abundance (about 54%) is observed at the sample surface. According to Figs. 6 and 7 there are three specific depth regions: 1) from zero to 80–100 nm, 2) from 100 to 250 nm, 3) deeper than 250 nm. Changes in isotope composition are more appreciable in the surface layers, where the rising implanted ion concentration (maximum is reached at the depth about 100 nm) has been observed (Fig. 6). The region of sharply decreasing implanted copper concentration in layers 120–250 nm corresponds to the isotope natural abundance, approximately.

A diffused "tail" of the implanted copper profile corresponds to the region, where the isotope composition coincides with the natural one. Thus, the maximum violation of isotope composition occurs in the region of maximum energy loss of implanted ions and maximum accumulation of implanted copper ion concentration. Fig. 8 shows analogous curves for the dose $2 \cdot 10^{16}$ ion·cm^{-2}. Comparing Figs. 7 and 8 we can see that the layer-by-layer mode of isotope composition does not change with the dose increasing although, for greater doses, the isotope composition change occurs at greater depths. Probably, it is due to increase in the total implanted copper concentration and its increase with depth is a result of radiation stimulated diffusion. This experiment was repeated at an ion implanted dose of $2 \cdot 10^{17}$

ion·cm^{-2} and pressure of 4·10^{-2} Pa. The copper isotope composition transformation effect did not change in general, but deviations in the copper isotopes implanted profiles have been found (Fig. 8). They become narrower, gathering towards the sample surface.

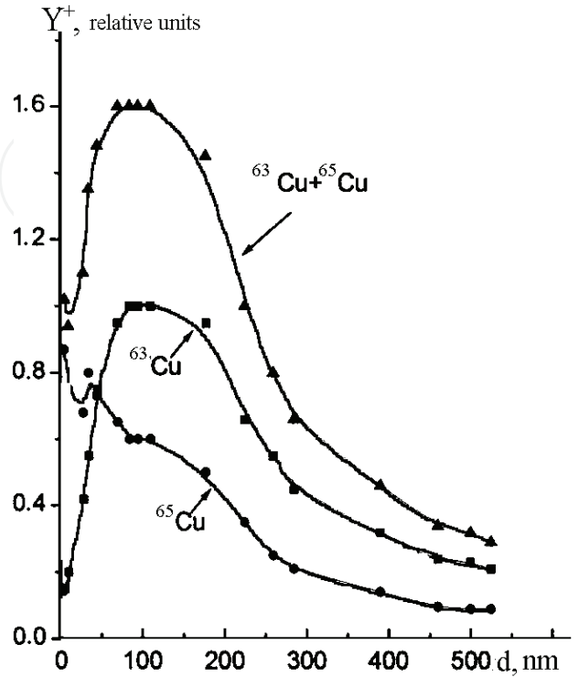

Fig. 6. The ^{65}Cu and ^{63}Cu depth distribution for a nickel sample, and summed ^{65}Cu+ ^{63}Cu profile.

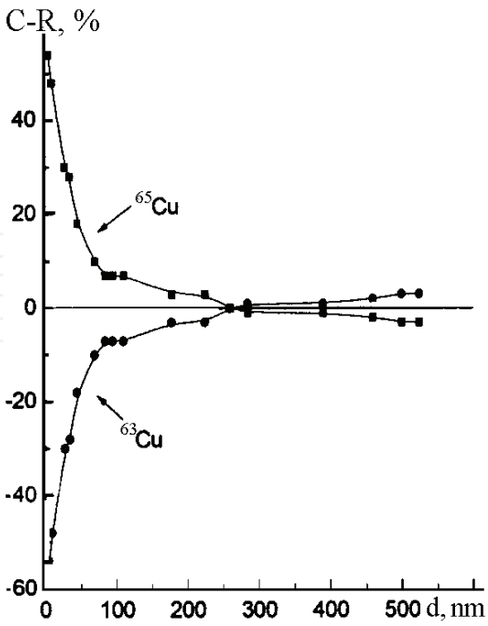

Fig. 7. Layer-by-layer deviations of the copper isotope concentration (C_i) from the natural abundance (R_i). Implantation dose is 2x10^{17} ions cm^{-2}.

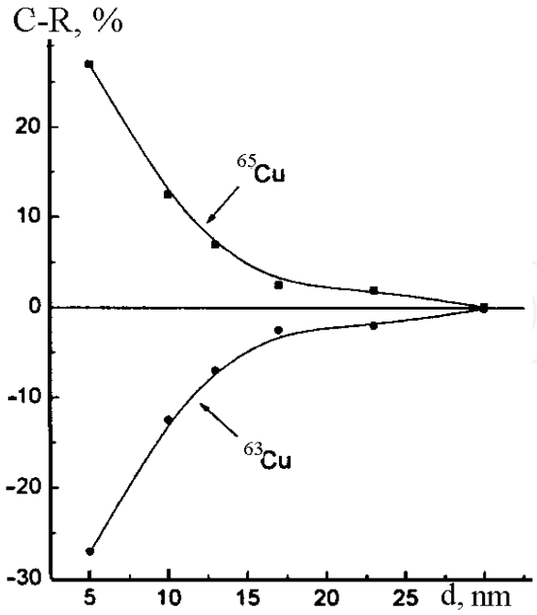

Fig. 8. Layer-by-layer deviations of the copper isotope concentration (C_i) from the natural abundance (R_i). Implantation dose is $2 \cdot 10^{16}$ ions·cm^{-2}.

Traditional diffusion mechanisms cannot explain the implanted copper isotope composition transformation. It is known that the ratio of isotope diffusion coefficients is inversely proportional to the square-root of their mass ratio: $D(^{63}Cu)/D(^{65}Cu) = (65/63)^{1/2} = 1.016$. However, the effect observed is several times greater.

2.2 The isotope effects during hydrogen saturation of materials

2.2.1 Massive metal samples of palladium and titanium

In table 1. are shown the data on a modification of the isotope composition of a massive (not thin-film) palladium samples after its saturation by the electrolytic expedient with use of electrolyte LiOD+D_2O (Chernov, Nikitenkov et. al., 2000).

The samples	Concentration of *i*-th isotope in an intermixture of isotopes, %				
A.m.u. of isotope	**104**	**105**	**106**	**108**	**110**
Natural intermixture	10.0	22.2	27.3	26.7	11.8
The initial sample	10.8	23.5	28.6	25.2	11.8
After saturation	16.4	25.0	21.4	22.9	14.3
Diversion from the natural	6.4	2.8	-5.9	-3.8	2.5

Table 1. Isotope composition of a palladium after saturation by a deuterium on observed datas on 10 samples (after surface refining by a sounding beam).

A procedure of the isotope compositions research was used the same what in part 2.2.2. From the Table 1 follows, that the isotope composition noticeably varies in surface layers of the palladium samples at electrolytic saturation by deuterium.

Fig. 9 shows a deviation of the content for the palladium isotopes in the course of the electrolytic saturation of a palladium and with an additional neutron exposure (Lipson, Maili et. al., 2003). In the Fig. 9: $\delta N=C-C_{ini}$, where C – the isotope concentration after and C_{ini} – before saturation.The purpose of the work was the determination of influence of mechanical stress on allocation of palladium isotopes. Mechanical stress in samples formed by both deuterium charging and an exposure by thermal neutrons.

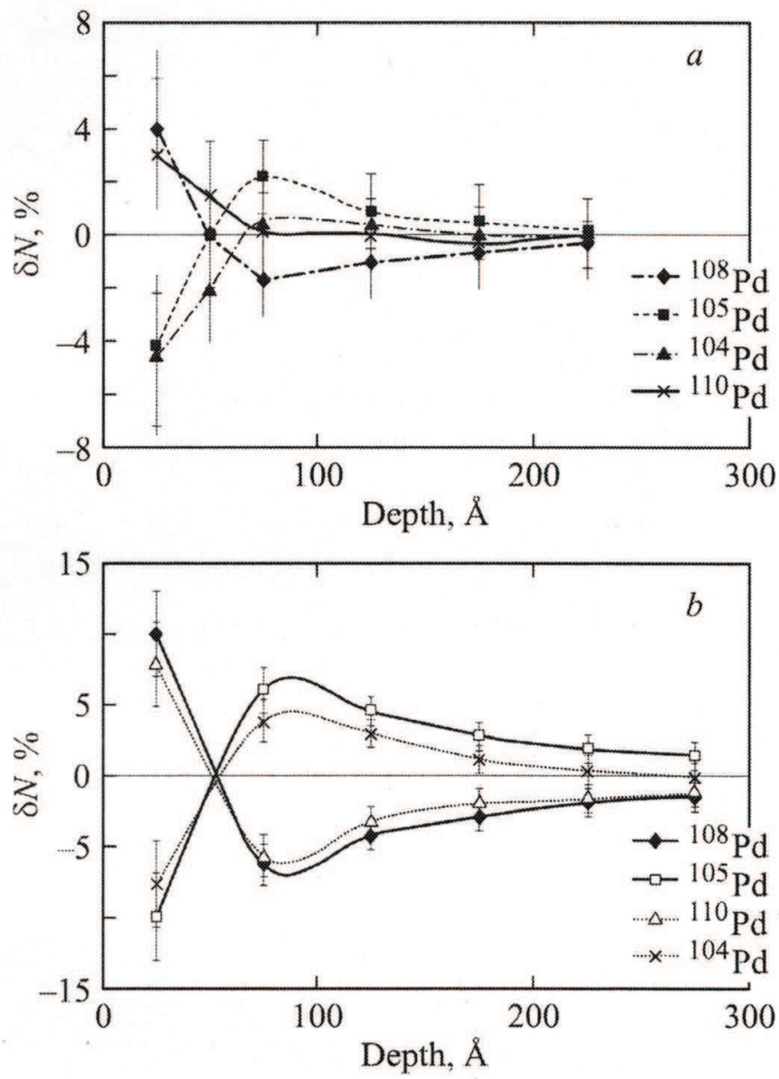

Fig. 9. Level-by-level diversions δN of the isotope concentration ^{104}Pd, ^{105}Pd, ^{108}Pd and ^{110}Pd as a result of a palladium samples saturation by deuterium: a - the sample subjected to an electrolysis within three days in the conditions of a natural neutron hum, b - the sample subjected to an electrolysis within three days at a simultaneous exposure by thermal neutrons (Lipson et al, 2003).

The deuterating of palladium samples made by electrolytic method in the 1 M NaOD solution at a cell with the parted anode and cathode spaces. Current density of electrolysis I_e=30 mA/cm^2; electrolysis time 1−3 days at room temperature. Composition of PdD_x

deuteride after the termination of an electrolysis: 0.72 <x <0.80. An exposure of samples be thermal neutrons with energy E_n=60 meV energy and Φ_n=200 n/s·cm² fluence made directly in the course of an electrolysis. After an electrolysis were measured a macroscopic buckling of the samples *l* and the residual plastic strain ε_p. It has been obtained, that at electrolysis in the conditions of a natural neutron hum average values of these parameters are equal $\langle l \rangle$=1.5 cm и $\langle \varepsilon_p \rangle = 3.0 \cdot 10^{-3}$. At the electrolysis in the presence of neutrons the straining parameters is a lot of above: $\langle l_n \rangle$=5.0 cm, $\langle \varepsilon_{pn} \rangle = 1.3 \cdot 10^{-2}$. The studying of the isotopic composition of the deuteride palladium samples was made by SIMS method on the CAMECA IMS 5f devise.

Analogously to a palladium there is a modification in the isotope composition in near-surface layers of the titanium at saturation by deuterium. In Table 2 and Fig.10 are shown the deviation from natural abundances for titanium isotope concentrations at saturation of titanium samples by deuterium (Chernov et al, 2000).

From Table 1 and Fig. 9 taking into account differences in experiment techniques reveals that in both independent experiments made by different authors, on different procedures of a sample preparation and effects examination follows that results are gained the similar.

Isotopies a.m.u.	Saturation dose, mA·min·cm^{-2}			
	4500	6000	12000	30000
	Maximum diversions, %			
	Large crystalline (LC)			
46	0.6	0.2	0.7	1.2
47	1.4	2.8	3.0	8.0
48	-2.0	-3.0	-3.7	-9.2
Submicrocrystalline (SMS)				
46	1.1	1.2	1.3	1.5
47	1.2	1.3	1.5	3.0
48	-2.3	-2.5	-2.8	-4.5

Table 2. The maximum deviations (from initial) in contents of the titanium isotopes in near surface area on two modifications of titanium samples depending on a dose of their saturation.

In the end of this partition we will descript some possible mechanisms of isotope separation (Lipson, Maili et. al., 2003) which can be responsible for given result.

Authors (Lipson et al, 2003) have viewed possible models of isotope separation for samples which similar viewed here (Fig. 9, 10; Tab. 1, 2). Thus for a palladium the following experimental quantities of effects are accepted (on the average): on depth h>100 Å concentration of ^{108}Pd isotope decreases and a ^{105}Pd isotope is increases by 5 % (for a pair ^{110}Pd–^{104}Pd on the average by 4 %). On this basis a factors of the full enriching are calculated according to (Kaplan, 1955).

$$A = \frac{N_F / (1 - N_F)}{N_I / (1 - N_I)}, \tag{5}$$

where $\langle N_F \rangle$=0.265 and $\langle N_I \rangle$=0.225 — average concentration, accordingly, ^{105}Pd and ^{108}Pd. From here follows $-A_1$=1.24. Analogously for a pair ^{110}Pd–^{104}Pd $-A_2$=2.55.

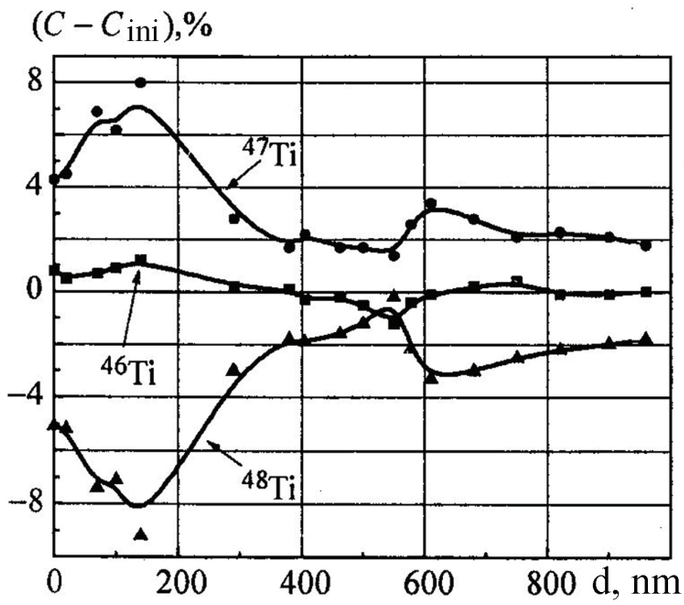

Fig. 10. Level-by-level distributions of the titanium isotope concentration in near-surface field of the large crystalline titanium after the electrolytic saturation by a dose of 30 000 mA·min·cm^{-2}.

On the basis of the gained results and calculations by (5) authors conclude that the diffusive model of isotope separation in this case does not work. Therefore it is supposed, that in a near-surface layers of the sample there are others, more effective reasons of isotope separation. As objects of such reasons can be the screw dislocations, dislocation loops or the spiral steps organized at cross of screw dislocations with a sample surface (Poluhin et al, 1982). If the rotation of such sites of the linear flaws happens with a velocity close to a sound velocity in Pd, than such objects can serve effective „nano-centrifuges" in which there is a hydrogen isotope separation. Really, a simple factor of partitioning α for such centrifugal machine is spotted as (Kaplan, 1955):

$$\alpha = \exp\left[\frac{(M_2 - M_1)(v_s)^2}{2RT}\right], \tag{6}$$

where v_s - the effective velocity of rotation accepted to an equal half of a sound velocity v_0; R – the gas constant; T — temperature. According to (6), for a pair ^{108}Pd−^{105}Pd —α =2.60 and for a pair ^{110}Pd−^{104}Pd — α =6.50. As A = α_s an isotope separation rather efficiently in case of a nano-centrifuging also it can be realized in one stage (s≤1) in a layer h <50Å. Notice that at isotope separation by a centrifuging method heavy isotopes move to rim of rotation (opposed to diffusive method) whereas a light isotopes will remain on the spot, i.e. its captured by a dislocations. Therefore the surface will be enriched by heavy (mobile) isotopes and depleted by light isotopes (related to a kernel of dislocations). It is necessary notice that the discovered effects of isotope separation can be expressed much more clearly on more major depth for light impurities in metals (Wilson et al, 1989). As impurities tend to a segregation exclusively in areas of concentration of internal stresses, referred an isotope separation models are most applicable to diffusing impurity atoms.

2.2.2 Thin-films systems

While studying (Chernov et al, 1998, 1999, 2000), (Nikitenkov et al, 2004, 2006), (Larionov et al, 2010) the isotope effects by hydrogen saturation we used the secondary ion mass spectrometry (SIMS) method to analyze the samples of bulk titanium (having various crystal structure), palladium, and thin film Ti/Al and Ti/ceramics structures. In all cases, at sufficiently large saturation doses appreciate deviations from the natural isotope abundance were seen in the surface layer both for the matrix elements and for the introduced admixtures.

Ti/Al and Ti/ceramics structures have been gained by a method vacuum magnetron depositions on the cleansed aluminum and ceramics surfaces. The thickness of titanium films made 0.4 microns, a thickness of aluminium substrates - 50 microns and ceramics substrates - 1 mm. Saturation of structures by the hydrogen isotopes was made by the electrolytic method at use it as the cathode. Electrolyte $LiOD+D_2O$ and $LiOD + (1/2)\ D_2O + (1/2)\ H_2O$ were used current density of electrolysis from 15 to 100 мА/см²; a time of saturation from 3 till 10 h.

Fig. 11, 12 shows the experimental data on a titanium-aluminum system before and after hydrogen saturation in $D+(1/2)D_2O+(1/2)H_2O$ electrolyte. The Y coordinate represents quantities proportional to the absolute yield of secondary ions. The film surface and the "film-substrate" interface change appreciably during the saturation. The regularities found are as follows.

a. D, H, Li, and Ti compounds are produced at the film surface. While sputtering through the depth of 200–300 nm (Fig. 12), the molecular LiD^+ and LiH^+ ions are found in the mass spectra of a saturated sample and a decreasing Ti^+ ion yield is observed (Fig. 11);
b. An isotope effect on the molecular ions yield is observed (Fig. 12). The Li_xD_y and Al_xD_y compounds are located nearer to the sample surface than the Li_xH_y and Al_xH_y compounds. This holds for the sample surface as well as for the transitional film-substrate region.

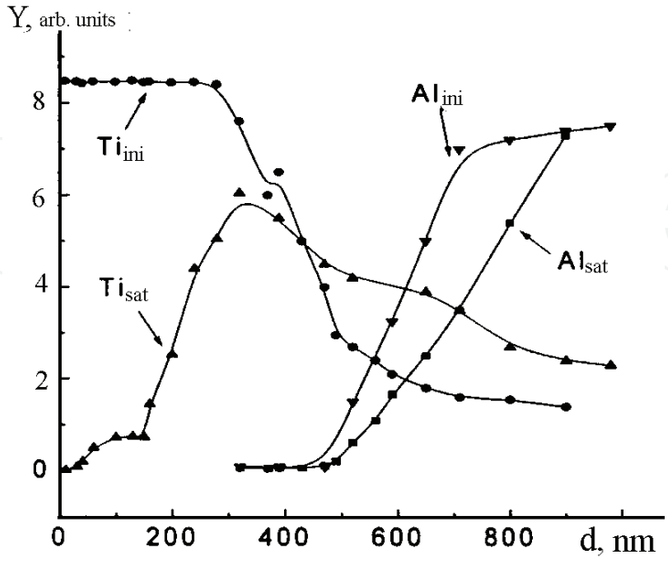

Fig. 11. Titanium and aluminum profiles of Ti/Al system before (ini) and after (sat) its electrolytic saturation by hydrogen isotopes.

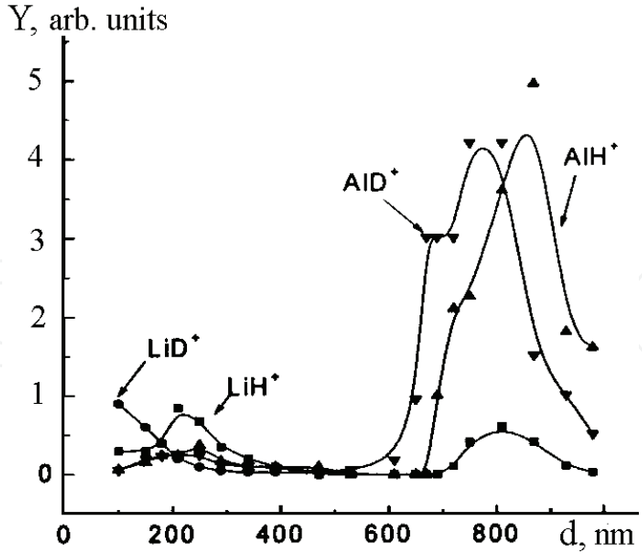

Fig. 12. Profiles of hydrogen and deuterium compounds after electrolytic saturation of the Ti/Al system by hydrogen isotopes.

Figs. 13 and 14 illustrate the appreciable deviations of lithium isotope concentration from its natural abundance in a Ti/Al system after saturation by the hydrogen isotopes. Fig. 11 shows the Li isotope profile. The maximum quantity of lithium is observed in the film formed on the titanium surface. In the film-substrate interface there is a plateau, and there is a recession at the point where the probe beam enters the aluminum substrate. At the depth 600–700 nm (the region previous to the region of AlH, AlD, and LiH ions maximum yield), a sharp peak in the ^{6}Li ions yield sharp peak is observed. This is a violation of the natural isotope abundance.

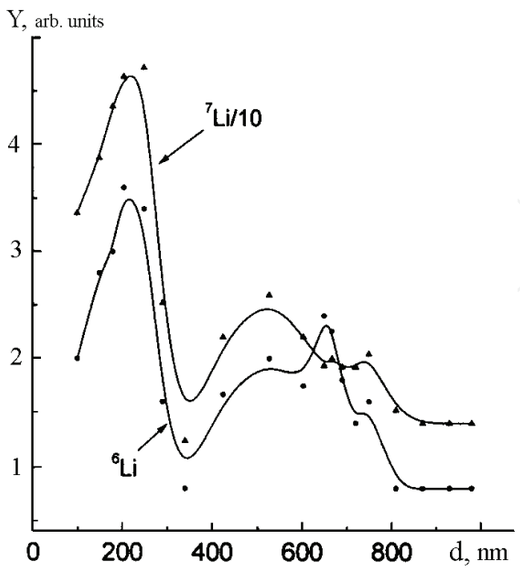

Fig. 13. The layer by layer profiles of the secondary lithium ions yields from the Ti/Al system after its saturation by hydrogen isotopes.

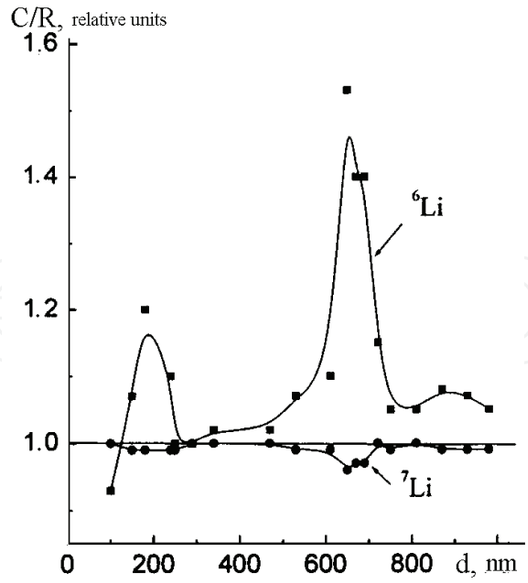

Fig. 14. The layer by layer (normalized to the natural occurrence) lithium isotope composition in the Ti/Al system, saturated by hydrogen isotopes.

In order to find the isotope ratio along the depth, the intensity ratio of $I_{(^{6}Li^{+})}/I_{(^{6}Li^{+}+^{7}Li^{+})}$ and $I_{(^{7}Li^{+})}/I_{(^{6}Li^{+}+^{7}Li^{+})}$ for all experimental spectra were measured. The quantities measured were divided by the corresponding tabulated isotope natural abundances. The results are shown in Fig. 14. It follows that, for ^{6}Li, a maximum excess above the natural abundance is observed.

Fig. 15 shows an example of the change in isotopic composition of a titanium film on ceramic, i.e., of the primary element in the film after saturation with a total dose of 12000 mA min cm^{-2}. In the case of a titanium film on aluminum, these differences (Fig. 15) are more obvious.

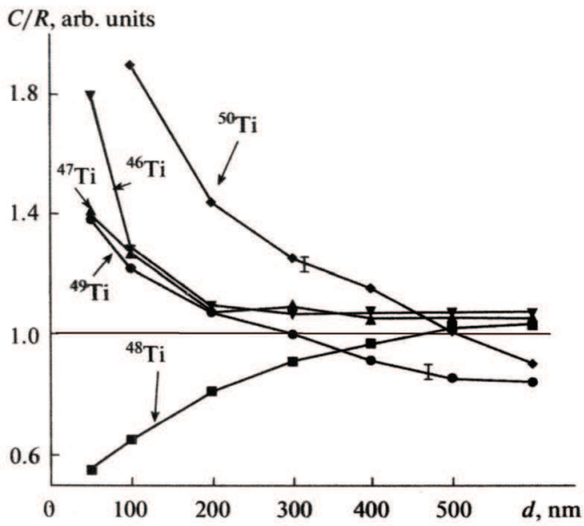

Fig. 15. Layer–by-layer difference in the relative concentrations of titanium isotopes after electrolytic saturation of the Ti/ceramic system.

This is apparently due to quite effective interdiffusion in the metal–metal system compared to that in the metal–ceramic system.

We will consider the observed effects in the lithium isotope separation (^{6}Li and ^{7}Li). On the basis of the theory and practice of isotope separation (Larionov, 2010), we will distinguish three possible processes leading to lithium isotope separation in the circumstances underconsideration: distribution with respect to mobilities in ion transport to the cathode; thermodynamic exchange in the solution–metal cathode system, specifically isotope diffusion in the cathode matrix; and lithium ion diffusion stimulated by hydrogen ions in the cathode metal. This last effect is corroborated by a rather high value of the diffusion coefficient in the cathode materials ($D=3\times10^{-9}$ cm^2/s). The separation factor for lithium isotopes with respect to nobilities does not exceed 1.003–1.006, and thus this process has little influence on the magnitude of the observed effect. We will consider the steps in the separation process, which most likely lead to isotope effects (from here on, isotope effect is understood to mean the difference in the lithium isotope concentration from that in the original composition). As the means for analyzing the effect of isotope separation based on thermodynamic exchange, we will use an estimate of β-factors of isotopes of the same metal (the β-factor is the ratio of the statistical sums over the states of the isotopic forms of molecular complexes). In this case the isotope effect or separation factor is equal to β-factor of the electrolyte/β-factor of the cathode metal.

Lithium ions in solution contain hydration layers. According to structural investigations, the coordination number for lithium ions in the primary layer, as well as in the secondary layer, is equal to 4; i.e., the total number of water molecules can be more than 8, depending on the lithium ion concentration in aqueous solution. As a lithium ion is implanted in the metal, its hydration shell is completely destroyed, and without this shell, the lithium atom forms a characteristic defect in the matrix of the primary metal (cathode). The free energy difference (^{6}Li and ^{7}Li) in the metal matrix is equal to

$$\Delta F = -kT\beta(Me), \tag{7}$$

where k – Boltzmann constant, T – absolute temperature, and β(Me) – β-factor of lithium isotopes in the metals.

$$\beta(Ti) = \exp\left[\frac{1}{2}kT\ln\left(\frac{K'}{K}\right)\frac{m}{m^*}\right] + kT\left\{\begin{array}{l}\dfrac{1}{24}\left[\dfrac{K}{K^*}\left(1+\dfrac{m}{m^*}\right)-1\right]\text{x} \\ \text{x}\left\{\left(\dfrac{\hbar\omega_p^2}{kT}\right)^2 - \dfrac{1}{2880}\right\}\left[\left(\dfrac{K'}{2K}\right)^2\left(\dfrac{m}{m^*}+\dfrac{m^2}{m^{*2}}\right)\right]+\text{N}\end{array}\right\}, \tag{8}$$

were $N = \dfrac{1}{8}\left(1+\dfrac{K'}{K}\right)^2 - \dfrac{1}{4}\left(\dfrac{\hbar\omega_p^2}{kT}\right)^4 + \cdots$

In these expressions: K, K' – force constants of the isotopic bond in the metal matrix, m, m* masses of the light and heavy isotopes, respectively, implanted in the metal matrix (electrode), and ω_p – vibrational frequency of the matrix–electrode lattice. Equation (8) was obtained from the formal apparatus developed for defects in crystals (Maradudin et al,

1965). Defect interaction in the "implanted metal–cathode matrix" structure can be estimated from the isotopic change in the vibration frequency of "defects"–atoms (^{6}Li and ^{7}Li). The calculated value for the isotopic shift in frequency is about 0.7–0.9 cm^{-1}. From Eq. (8), the β-factor of lithium isotopes in titanium is 1.088. The β-factor of hydration complexes of lithium isotopes is calculated from the expression:

$$\beta = \prod_{i=1}^{n} \left(\frac{U_i^*}{U_i} e^{-\frac{U_i^*}{U_i}} \cdot \frac{1 - e^{-U_i}}{1 - e^{-U_i^*}} \right)^{1/2}, \tag{9}$$

where n – the number of equivalent atoms of a given isotope available in the molecule or complex under consideration, and U_i, U^*_i – the vibrational frequencies of molecules with the light and heavy lithium isotopes, respectively $U = \frac{\omega ch}{kT}$, h – Planck's constant, ω - the vibrational frequency of an isotope in a molecule (complex), c is the speed of light in a vacuum, and T is the absolute temperature. The vibrational frequencies of isotopic lithium ions in the molecule of an aquo complex were calculated by solving the secular equations. The β-factor of a lithium aquo complex with four molecules of water is 1.136. The effect of the secondary hydration layer on the value of the β-factor is shown in the Table 3. We note that a sharp change in the β-factor is typical for 1–4 molecules of water, while it changes smoothly for n = 5–8. Further increase in the number of water molecules in the hydration sphere does not lead to a change in the β-factor. Thus, the significant change in the isotopic composition (isotope effect) of lithium implanted in the cathode can be explained by the destruction of the hydration layer as the ion enters the metal. Furthermore, this effect increases with the induced diffusion of lithium atoms through the cathhode in the flow of hydrogen atoms (Fig. 3, depth of 700 nm). This is supported by the fact that there is almost no hydrogen in the aluminum substrate, while its concentration is significant in the titanium. Isotope effects occurring during SIMS analysis (see part 2.1 of this chapter) can somewhat decrease the observed isotope effect during lithium implantation in the cathode. In a series of articles devoted to the electrolytic implantation of heavy and light hydrogen in different metals from solutions, the authors suggest that the change in isotopic composition in the metal–cathode (titanium) in which implantation took place, in impurities in the cathode, and in the ions responsible for electrolyte conductivity was the result of cold nuclear transmutation (Mizuno et al, 1996), (Beaudette, 2002). However, our experimental data point primarily to the effects of isotope disproportionation, which accompany electrolytic ion implantation in the cathode.

nH_2O	5	6	7	8
β - factor	1.146	1.155	1.162	1.170

Table 3. Calculated values of the β-factor for aquo complexes of lithium isotopes (n represents the number of water molecules in the aquo complex).

So, we have established that the electrochemical implantation of lithium in metals and composite materials is accompanied by isotope separation. This is caused by both a thermodynamic effect and the diffusion processes involving hydrogen, which accompany the process of implantation.

2.3 The isotope effect by thermo diffusion of copper atoms in nickel

The isotope effect during thermo-diffusion of copper atoms in nickel under the conditions of material creep has been studied (Puchkareva et al, 2002). When this condition holds, grain boundary diffusion of copper atoms in nickel occurs in conditions an external electric field and temperature-time non-stationary regime under an appreciate inner strain (osmotic pressure). According to these conditions (especially, the inner strain), the situation when the grain boundary diffusion occurs, is analogues to that for hydrogen saturation, because the hydrogen charge in solid matrix is accompanied by considerable strains.

Fig. 16 shows the isotope composition depth distribution of the copper atoms in nickel after diffusion and creep occurring over four hours at a temperature 600 K and strain of 10 kg/mm². An analogous isotope composition change was registered for other samples. Under these conditions, appreciable isotope redistribution is observed. It has been shown that there is a qualitative resemblance of this effect with the titanium isotope depth composition change while hydrogen saturates a titanium-ceramic system and bulk titanium and palladium samples. In all cases, the effect happens only in the near-surface layers (diffusion zone). In an isotope mixture, a concentration decrease of the most widely distributed isotope in the diffusion surface zone has been observed. A specific depth (about the influence of the surface on the diffusion redistribution of isotopes. The Cu/Ni samples, which were not influenced by an external force, do not show an isotope composition change.

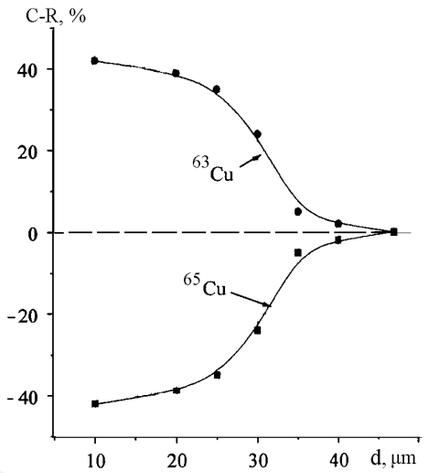

Fig. 16. Lateral view of the isotope composition diversions from natural of copper in nickel after diffusion in conditions of a creep.

2.4 Isotope effects during action of chemical active solutions on the solid surface

The influence of electrochemically activated sulphuric acid solutions on silicon wafers which are used for integrated circuits has been studied (Nikitenkov et al, 1993). The sulphuric acid solution was activated in an electrolyzer with a platinum anode and graphite cathode. The mirror silicon wafer surfaces were treated by an activated solution in a fluorine plastic cup at room temperature and various time intervals. After this procedure, the wafers were analyzed by secondary ion energy mass spectrometers. The experimental data on the silicon composition on the silicon wafers after various treatments are shown in Table 4. The samples are polished silicon wafer (up to mirror finish). Treatment 1 – was in a mixture H_2SO_4:H_2O_2.

Isotope A.m.u. Si	Natural occurrence %	Silicon isotope concentration, %		
		Initial sample	Treatment 1	Treatment 2
28	92.27	84.4	72.8	76.9
29	4.68	12.0	23.7	19.8
30	3.05	3.6	3.5	3.3

Table 4. Silicon isotope concentration in a Si^+ flux while sputtering the silicon target surface after various treatments.

Treatment 2 – was in electro-chemically activated H_2SO_4. The Table shows that the mechanical buffing and subsequent chemical treatment caused an appreciable increase in the secondary heavy ion yields.

This increasing is not due to the isotopic effect in the secondary ion emission (part 2.1 of this chapter), because this effect decreases the heavy ion yield. The peak overlapping (^{28}SiH upon ^{29}Si) and ($^{28}SiH+^{29}Si$ upon ^{30}Si) can partially be responsible for this increase. However, such an explanation contradicts the Table 1 data: the ^{29}Si concentration after mechanical and chemical treatment is several times greater than the natural one, while the ^{30}Si concentration is only 15–20 % greater. If this effect were due to the peaks overlapping, the opposite behaviour should be observed. We assume that the surface treatment is responsible for the natural isotope concentration violation. This violation mechanism (after chemical treatment) is probably caused by the isotopic displacement of the silicon valence electron energy levels analogous to the ionization level shift in the secondary ion emission.

Another isotopic effect while treating the sample surface by chemical solutions consists in changing the $LiNbO_3$ crystal surface after proton-ion doping. The studies (Sergeev, et al, 1991) were made using energy-mass-spectrometry method. In the proton-ion doping process, the sample surface is treated in a benzoic acid (C_6H_5COOH) melt with doping ingredients (salts or oxides) at the temperature 200–440 ^oC during the time interval up to 10 hours. Table 2 shows the lithium isotope concentrations in the secondary lithium ion flux while adding various doping ingredients.

Lithium isotope a.m.u	Natural occurrence, %	Doping agent					
		Be	Ca	Mn	Ni	Sr	Ba
		Lithium isotope concentration , %					
6	7.4	4.8	5.7	5.5	6.5	6.8	6.2
7	92.6	95.2	94.3	94.5	93.5	93.2	93.8

Table 5. The lithium isotope concentration in the secondary Li^+ flux while sputtering the $LiNbO_3$ crystal surfaces doped by various elements.

The Table 5 data are similar to those ones in the Table 4: the enrichment of the lithium secondary ion flux by the heavier lithium isotope is observed. The effect tends to grow with the doping ingredient mass. In the Table, they are arranged in order of their mass. As for silicon samples (Tab. 4), the natural abundance violation cannot be explained by the experimental errors. While proton-ion doping, the doping atom replaces the lithium or niobium atom in $LiNbO_3$ lattice, thus the effect is probably caused by the isotopic displacement of valence electron energy levels.

3. Conclusion

The experimental data presented may be divided into three groups in accordance with the physical process.

The first one is associated with surface sputtering, surface scattering, and ion implantation. The main features observed in these processes is an enrichment of surface isotope composition by heavy isotopes reflected or sputtered from the surface. The features of atomic collision and electron interaction in the atom-surface system are responsible for these regularities.

The second one is associated with hydrogen saturation metals and thermo diffusion from external sources. In this case the main features are a decreasing concentration of the most prevalent isotope in a diffusion surface zone. This is caused by an entropy concentration levelling. For the thin-film systems, the accumulation of lighter isotopes in defect regions is due to preferential pinning of the smaller radius atom on defects.

The third one is less studied, and is associated with the chemical reactions on the surface and in the surface layers. The main features, as in the first group, are the enrichment by heavier but not always the heaviest isotopes: ^{29}Si (Tab. 4) and ^{7}Li (Tab. 5). That is in this case the effect is observed for nuclear which possess by the magnet moment (nuclear do not possess even values of a charge and mass number). Therefore, the mechanism of this effect is probably fractionation of nuclear-isotopes on a nuclear magnetic moment by chemical reactions (Buhanchenko A.L., 2007).

4. References

Aksenov, A.I.; Bugaev, S.P.; Emelyanov, V.A.; et al. (1987). Deriving of the wide-aperture ions beams of metals. *Devices and experimental technique;* No 3, pp. 139–142, ISSN 0032-8162 [Russian].

Buhanchenko A.L. *New isotopy in chemistry and biochemistry.* (2007). Moscow. Nauka. ISBN 5-02-035617-4 [Russian].

Galimov E.M. (1981). *The nature of a biological fractionation of carbon isotopes.* Moscow. Nauka. ISBN 5-02-035617-4 [Russian].

Chernov, I.P.; Nikitenkov, N.N.; Puchkareva, L.N.; et al. (1999) Change in isotopic composition of metals enriched in hydrogen. *Russian Phys. Journ.*, No 4, pp. 61–65, ISSN 0367-6755 [Russian].

Chernov, I.P.; Nikitenkov, N.N.; Puchkareva, L.N.; Kolobov, Yu.R. (1998). Isotopic Composition of Metals at Deuterium Charge *Proceedings of the seventh international Conference. Cold fusion* (*ICCF-7*). Vancouver. pp. 441–446 [Copyright 1998 ENECO. – Inc. Salt Lake City, Utah, USA]

Chernov, I.P.; Nikitenkov, N.N.; Krening, M.; Baumbach, H. (1999). Changes in lithium isotopic composition in hydrogen-enriched Ti/Al systems. *Russian Phys. Journ.*, Vol. 42. – № 11. – pp. 947–951. ISSN 0021-3411

Chernov, I.P.; Nikitenkov, N.N.; Puchkareva, L.N. et al. (1999). Change in isotopic composition of metals enriched in hydrogen *Russian Phys. Journ.*, Vol.42, No 4, pp.427–430. ISSN 0021-3411

Chernov, I.P.; Nikitenkov, N.N.; Kroning, M.; Baumbah, H. (2000). Change in lithium isotope composition in thin-film structures at hydrogen charge. *Izv Russ Acad Sci. Phys*., Vol.64, No11, pp.2181–2185, ISSN 0367-6755 [Russian].

Chernov, I.P.; Nikitenkov, N.N.; Kröning, M.; Baumbah, H. (2000). Investigation of the modification mechanism of metals isotope composition at hydrogen charge. *Proc Tomsk Polytech Uni.,* Vol. 303, Is.3, pp.62–71, ISSN1684-8519 [Russian].

Erikson, R.I.; Smith, D.P. (1975). Electronic processes in low-energy ion-surface scattering. *Phys Rev Lett,* 34, pp. 297–300 ISSN 0031-9007.

Gangrskiy, Yu. P.; Markov, B.N. (1984). *Nuclei in laser beams*. Ed. Kutuzova, K.A.; Moscow: Knowledge, 64p. ISSN 0373-2444. [Russian].

Gnaser, H. & Hutcheon, J.D. (1987). Velocity-dependent isotope fractionation in secondary ion emission. *Phys Rev B*; Vol.35, No1, pp.877–879. ISSN 1098-0121.

Gnaser, H. & Hutcheon, J.D. (1988). Preferential emission of light isotopes in the initial stage of sputtering. *Surf Sci*; Vol.195, pp. 499–511. ISSN 0039-6028 .

Gnaser, H. & Oechsner, H. (1990). Isotopic mass effect in sputtering: dependence on fluency and emission angle. *Nucl Instrum Methods Phys Res;* B48, pp. 544–8. ISSN 0168-9002

Helbig, H.F. & Adelman, P.J. (1977). Isotope Effects in Ion-Scattering Double Spectroscopy. *J Vac Sci Technol*, Vol. 14, pp. 488–93. ISSN

Helbig, H.F. & Orvek, K. (1980). Isotope Effects in Elastic Ion-Surface Scattering; He^+ and Ne^+ on Solid and Liquid Ga. *J Nucl Instrum Methods*, Vol. 170, pp. 505–507.

Kaplan, J. (1955). Nuclear Physics. Addison-Wesley. Cambridge.Mass.

Larionov, V.V.; Nikitenkov, N.N. & Tyurin, Yu.I. (2010). Isotope Distribution in Electrochemical Ion Implantation in Metals and Composite Materials. *Russian Journal of Electrochemistry,* Vol. 46, No. 1, pp. 112–115. ISSN 1023-1935

Lipson, A.G.; Maili, J.H.; Kuznetsov, V.A.; Asami, N. (2003). Isotope separation of a palladium under the influence of the strong mechanical stresses originating at loading Pd-folg by a deuterium. *Soli-state physics*, V. 45, Is. 8, pp. 1345–1350.ISSN: 0367-3294(Russian)

Lorin, J.C.; Havette, A. & Slodzian, G. (1982). *Abstract of conference on secondary ion mass spectrometry.* Berlin: Springer, p. 140.

Maradudin, A; Montrell, E & Weiss J. 1965. The dynamic theory of a crystal lattice in the harmonious approach. Moscow. Mir, 362 p.

Mizuno, T; Ohmori, T & Enyo, M. (1996). Isotopic changes on the reaction products induced by cathode electrolysis in Pd. *Journal of New Energy,* V.1, No 3, p.31.

Beaudette, C.G. (2002). *Excess Heat. Why Cold Fusion Research Prevailed.* OAK GROVE PRESS, LLC. South Bristol, Maine, USA. 410p.

Nikitenkov, N.N.; Kositsin, L.G.; Markova, N.M.; Shulepov, I.A. (1987). About an isotope effect in the secondary ion emission. *Abstract of XVII international conference Interaction the Charged Particles with Crystals*, MSU, p. 110 [Russian].

Nikitenkov, N.N. (1987). Theoretical and experimental studies of the secondary ion distribution while sputtering the complex composition targets by the Kev ions. *The author's abstract of doc. phys-math. sci. thesis.* M. MSU; 17p [Russian].

Nikitenkov, N.N.; Kositsin, L.G.; Markova, N.M.; Shulepov, I.A. (1988). About an isotope effect in secondary ion emission. *The secondary ion and photon emission. Reports of All-Union seminar.* Charkov: ChSU; Part 1. pp. 69–71 [Russian].

Nikitenkov, N.N.; Chernova, E.E.; Markova, N.M.; et al. (1993). Estimate of inhomogeneity of impurities distribution on a silicon plates surfaces. *Surface. Phys Chem Mech*, No. 10, pp. 74–78 [Russian].

Nikitenkov, N.N.; Chernova, E.E.; Karbainov, Yu.A.; et al. (1996). Some regularity of a real surface silicon modification by electrochemically activation in solutions of sulphuric acid. *Surface. X-ray Synchrotron Neutron Stud,* No. 11, pp. 45–50 ISSN: 1027-4510 [Russian].

Nikitenkov, N.N.; Chernov, I.P. &Tyurin, Yu.I. (2004). Isotope effects at technogenic affectings on a solid surface. Part 1: *Proc Tomsk Polytech Uni,* V. 307, No2. pp. 9–14; Part 2: *Proc Tomsk Polytech Uni,*V. 307, No. 3, pp. 26–29. ISSN: 1684-8519 [Russian].

Nikitenkov, N.N.; Kolokolov, D.Yu.; Chernov, I.P.; Tyurin, Yu.I. (2006). SIMS investigations of isotope effects at a processed solid surface. *Vacuum,* V.81, Is.2, pp. 202–210. ISSN: 0042-207X.

Poluhin, P.I.; Gorelik, S.S.; Vorontsov, V.K. (1982). Physics basis of plastic strain. Moscow. Metallurgija, 584 p.

Puchkareva, L.N.; Chernov, I.P. & Nikitenkov, N.N. (2002). Modifications of isotope composition of copper at the ionic implantation in nickel. *Izv Russ Acad SciPhys*, V.66, No. 8, pp. 1219–22, ISSN: 0367-6755 [Russian].

Plekhanov V.G. (2003). Isotopic effects in lattice dynamics, *Successes of physical sciences* (Russian), V. 173, No 7, pp. 711–738. (For the English speaking reader *Physics–Uspekhi* 46 (7) (2003) ISSN: 1063-7869 (Print), 1468-4780 (Online))

Slodzian, G.; Lorin, J.C. & Havette, (1980). A. Isotopic effect the ionization probabilities in secondary ion emission. *J Phys Lett,* V. 41, pp. L555–558. ISSN: 0370-2693

Shapiro, M.H.; Haff, P.K.; Tombrello, T.A.; Harrison, D.E. (1985). Simulation of isotopic mass effects in sputtering *Nucl Instrum Methods Phys Res*; V. B12, pp. 137–145. ISSN: 0168-9002

Shimizu, N. & Hart S.R. (1982). Isotope fractionation in secondary ion mass spectrometry. *J Appl Phys*, V. 53(3), pp. 1303–1311. ISSN: 0021-8979

Shwarz, S.A. (1987). Measurement of the secondary ion mass spectrometry isotope effect. *J Vac Sci Technol*, V. A5(3), pp. 308–312. ISSN: 0734-211X

Smith, D.P. (1971). Analysis of surface composition with low-energy backscattered ions. *Surf Sci*, V. 25, pp. 171–191. 0039-6028, ISSN 0039-6028

Sergeev, A.N.; Bamburov, V.G.; Nikitenkov, N.N.; Shveikin, G.P. (1991). The Oxide Surface Proton–Ion Doping. *Soviet Union Science Academy Reports.* Sverdlovsk: Chemistry Institute Preprint; 90p [Russian].

Shukolyukov Yu. A. (1996). Star dust in the hand. *Soros Educat. Journ.* №7, pp.74-80 ISSN 1684-9876 [Russian].

Tolk, N.H.; Tully, J.C.; Kraus J. et al. (1976). Angular dependence of oscillatory structure in low-energy ion-surface scattering. *Phys Rev Lett*, V. 36, pp. 747–750. ISSN. 0031-9007.

Wilson, R.G.; Stevie, F.A.; MageeL.W. (1989). Secondary Ion Mass Spectrometry. A Practical Handbook for Depth Profiling and Bulk Impurity Analysis. J. Wiley, N.Y.

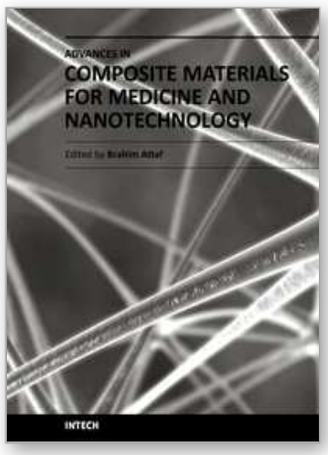

Advances in Composite Materials for Medicine and Nanotechnology

Edited by Dr. Brahim Attaf

ISBN 978-953-307-235-7
Hard cover, 648 pages
Publisher InTech
Published online 01, April, 2011
Published in print edition April, 2011

Due to their good mechanical characteristics in terms of stiffness and strength coupled with mass-saving advantage and other attractive physico-chemical properties, composite materials are successfully used in medicine and nanotechnology fields. To this end, the chapters composing the book have been divided into the following sections: medicine, dental and pharmaceutical applications; nanocomposites for energy efficiency; characterization and fabrication, all of which provide an invaluable overview of this fascinating subject area. The book presents, in addition, some studies carried out in orthopedic and stomatological applications and others aiming to design and produce new devices using the latest advances in nanotechnology. This wide variety of theoretical, numerical and experimental results can help specialists involved in these disciplines to enhance competitiveness and innovation.

InTech Europe
University Campus STeP Ri
Slavka Krautzeka 83/A
51000 Rijeka, Croatia
Phone: +385 (51) 770 447
Fax: +385 (51) 686 166
www.intechopen.com

InTech China
Unit 405, Office Block, Hotel Equatorial Shanghai
No.65, Yan An Road (West), Shanghai, 200040, China
中国上海市延安西路65号上海国际贵都大饭店办公楼405单元
Phone: +86-21-62489820
Fax: +86-21-62489821

IntechOpen